



Studying the Structural, Morphological, Optical, and Electrical Properties of CdS/PbS Thin Films for Photovoltaic Applications

Mustafa K. A. Mohammed¹

Received: 3 April 2020 / Accepted: 29 June 2020 / Published online: 6 July 2020
© Springer Science+Business Media, LLC, part of Springer Nature 2020

Abstract

The cadmium sulfide (CdS) and lead sulfide (PbS) materials have been chosen in order to boost solar energy conversion from ultraviolet region to the near-infrared (NIR) spectral region. These materials belonging to the II–VI group have suitable direct band gaps and in solar energy conversion. CdS and PbS layers are used as window and absorber materials, respectively, in solar cells. This paper presents structural, morphological, and optical properties of PbS and CdS thin films prepared by chemical spray pyrolysis at different temperatures as well as its photovoltaic performance. The X-ray diffraction results show the PbS films have cubic structure and CdS films have hexagonal structure. FESEM measurements reveal the films have homogeneous surfaces with spherical particles. Optical analyses exhibit the optical band gap redshifts as the substrate temperature increases. Illumination current density–voltage test of ITO/CdS/PbS/Au heterojunction with different thicknesses of PbS layer has been evaluated. The optimal results are obtained in ITO/CdS/PbS/Au solar cell where thickness of PbS layer is of 0.9 μm with maximum short circuit current, open circuit voltage, and fill factor as well as highest efficiency.

Keywords PbS/CdS thin film · Spray pyrolysis · X-ray diffraction · Semiconductor · Optical properties

Introduction

The ever-increasing power demand has pushed the research community to find more efficient, environmentally safely, renewable, and low-cost energy sources to replace the actual dominant oil and fossil fuel [1]. Because of the inexpensive development and the moderately high theoretical power conversion efficiency, thin-film solar cells are appearing as a highly interesting kind of renewable power sources [2]. They also have versatile features such as capability of multiple exciton generation, high stability against heat, and tunable band gap because of the quantum confinement effect [3]. PbS is a significant semiconductor compound material in the manufacturing of absorber layers for photovoltaic applications due to small band gap approximately from 0.36 to 0.42 eV, appropriate exciton Bohr radius of around 18 nm, and provides electrons and holes with efficient quantum confinement, driving to a raise in the absorption of the solar spectrum in the near infrared range [4]. These features make lead sulfide plays

significant role in the photovoltaic applications [5]. CdS thin films are regarded as one of the most important substances for solar cell applications [6]. It has wide band gap (2.5 eV) with high optical transmittance and high electrical conductivity [7]. For these reasons, CdS can be used as the window layer beside with other semiconductors such as CdTe, CIGS, and ZnO [8–10].

There are various routes for thin-film fabrication, for instance, chemical bath deposition (CBD) [11], spin coating [12], pulsed laser deposition [13], chemical vapor deposition [14], sputtering method [15], successive ionic layer absorption and reaction (SILAR) techniques [1], and chemical spray pyrolysis (CSP) [16]. The development of low-cost polycrystalline thin-film photovoltaic devices is significant for future power production. The CSP technique has been more attractive technologies, which are well suited for large area coating, low-temperature processing, simple, economical, and energy-effective approach for fabricating thin films of semiconductors [17]. CSP is particularly a precursor undergo to chemically react by spraying a solution into a substrate heated at elevated temperature, after that the precursors react to produce the demanded material [18].

This paper reports for first time the CSP method for preparing CdS thin film as window layer and PbS thin film as absorber layer for photovoltaic applications. The impacts of substrate temperature on structural, morphological, and

✉ Mustafa K. A. Mohammed
mustafa_kareem97@yahoo.com

¹ Technical Engineering College, Middle Technical University, Baghdad, Iraq

optical properties of the prepared films were investigated by XRD, FESEM, and UV-Vis spectroscopy, respectively. Also, photovoltaic properties of the ITO/CdS/PbS/Au solar cells were characterized by illumination with power of 50 mW/cm². The fabricated solar cell showed a significant enhancement of efficiency from 0.07 to 0.85% by increasing absorber layer thickness from 0.3 to 0.9 μm. The photovoltaic results are discussed and compared to the results reported in the literature.

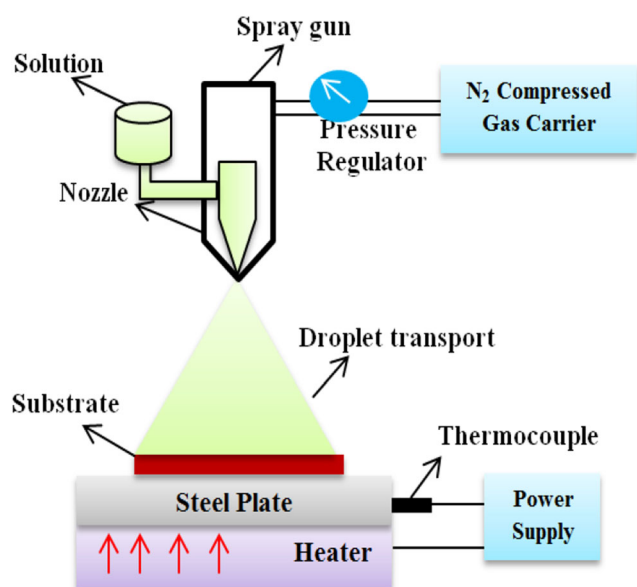
Experimental Part

Solution Preparation

A cadmium chloride (CdCl₂) and thiourea (CS (NH₂)₂) were used as precursor materials to deposit CdS thin film. The CdCl₂ and CS(NH₂)₂ were dissolved in deionized water in a separate manner, then mixing together at molarity of 0.02 M via magnetic stirrer for 30 min at room temperature. For PbS, lead nitrate (Pb (NO₃)₂) and thiourea were dissolved in deionized water at molarity of 0.05 M, then magnetically stirred for 20 min at room temperature.

Device Preparation

The ITO-coated glass substrate was used for depositing thin films. First, the slides were cut into small pieces with dimensions 1 cm × 1 cm and washed with acetone and hydrochloric acid (HCl, 20%), then placed in vacuum furnace at 50 °C to dry prior using. The PbS, CdS, and CdS/PbS thin films were grown on ITO/glass slides by utilizing the CSP route, as shown in Scheme 1. Briefly, the prepared solution was poured



Scheme 1 Chemical spray pyrolysis system

into the container of the nozzle and the slide was located on the heater to heat the slide to the desired temperature (200, 250, and 300 °C). The distance between the nozzle and the heated slide was maintained to be 30 cm. Then, the solution was sprayed in vertical type and the droplets of precursor were applied in good way on the slide for 30 s. After deposition, the slide was left to cool down to the room temperature [16]. To finish cell structure, a gold layer of thickness of 30 nm was performed as an Ohmic contact substance by a sputtering method, as presented in Scheme 2.

Characterization

Morphological features of prepared thin film were characterized by field emission scanning electron microscope (FESEM, ZEISS-SIGMA300), and the statistical distribution of the particle size was measured by using ImageJ software. UV-Vis spectroscopy (double beam, SolidSpec-3700i) was employed to determine the optical properties of prepared films. The optical absorption coefficient (α) was evaluated by utilizing following equation [19]:

$$\alpha = 2.303 \left(\ln \frac{1}{T} \right) \times \frac{1}{t}$$

where t is the film thickness and T is the transmission. The optical band gap (E_g) was determined by Tauc equation [20]:

$$\alpha = A(h\nu - E_g)^{\frac{1}{2}}$$

where A , h , and ν are a constant, Plank's constant, and the photon frequency, respectively. The X-ray diffraction technique (XRD, Philips PW 1840, $\lambda = 1.5406 \text{ \AA}$ from Cu-K α) was accomplished to study the structural properties of prepared films and compared with JCPDS reported data. From XRD data, the interlayer spacing (d) was determined by Bragg's law [21]:

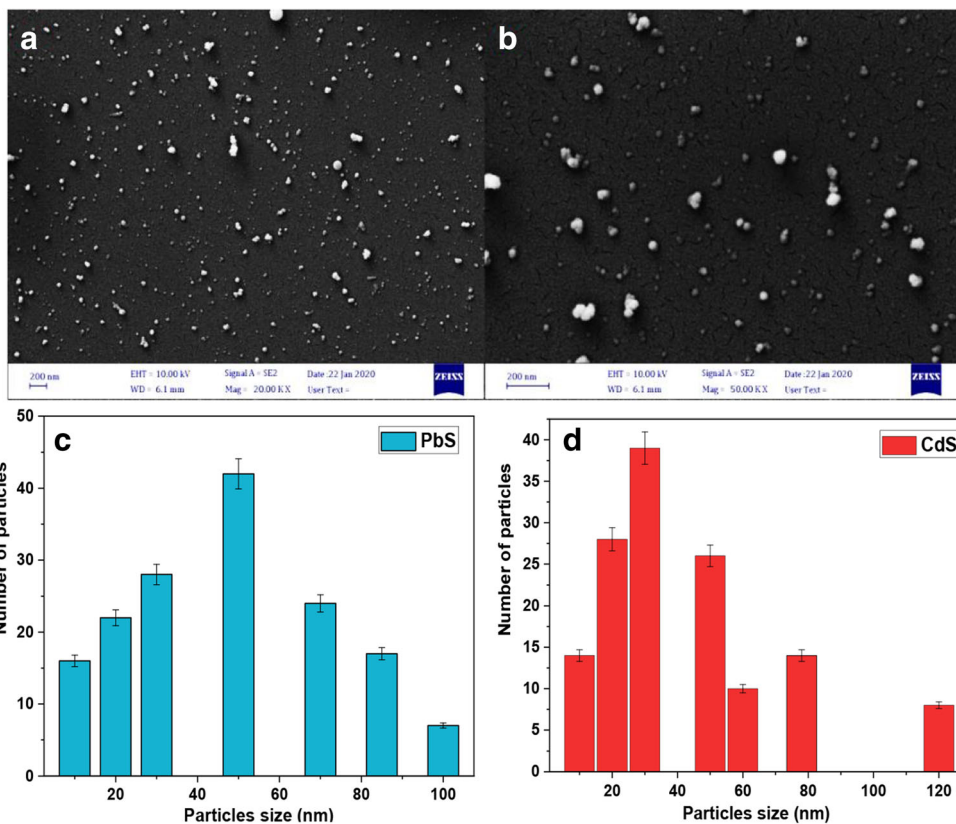
$$n\lambda = 2d \sin\theta$$

where n , λ , and θ are the order diffraction, X-ray wavelength, and diffraction angle, respectively. The Debye–Scherrer relation was accomplished to calculate the average crystallite size (L) of prepared thin films as follows [22]:



Scheme 2 ITO/CdS/PbS/Au solar cell system

Fig. 1 **a** FESEM for PbS, **b** FESEM for CdS, **c** particle distribution for PbS, and **d** particle distribution for CdS



$$L = \frac{K\lambda}{B \cos\theta}$$

where K and B are a constant (0.9) and full width at half maximum (FWHM), respectively. The cubic lattice constant (a) of the PbS thin film was calculated by using following relation [23]:

$$\frac{1}{d} = \frac{\sqrt{h^2 + k^2 + l^2}}{a}$$

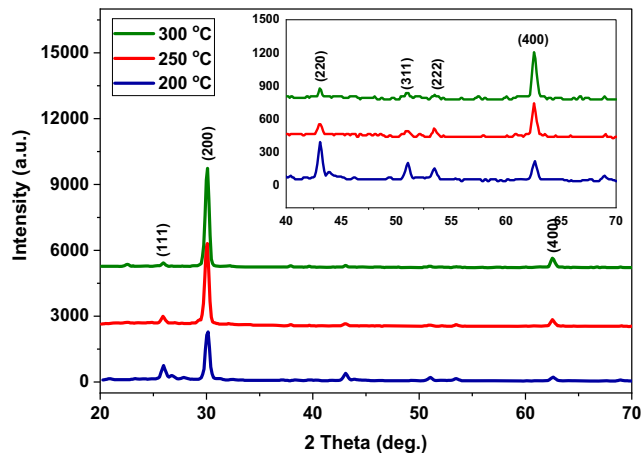


Fig. 2 XRD for PbS films prepared at different temperatures

where (hkl) are Miller indices. Also, the hexagonal lattice constants (a and c) of CdS thin film were determined by following equation [24]:

$$\frac{1}{d^2} = \frac{4}{3} \times \left(\frac{h^2 + hk + l^2}{a^2} \right) + \frac{l^2}{c^2}$$

Capacitance–voltage (C-V) measurements in the reverse bias manner were evaluated with a frequency of 100 kHz via a PM 6306 Programmable LRC meter supplied by Fluke. J-V characteristics were accomplished in the forward bias manner under illumination. A DC power supply (type L, voltage range from 0.1 to 5 V), a Keithley (602) electrometer, and halogen lamp (50 mW/cm^2) were used for this purpose. The thicknesses of PbS and CdS films were evaluated by laser interference and found to be 0.3, 0.6, and 0.9 μm for PbS and 150 nm for CdS.

Table 1 XRD parameters for PbS thin films

Temperature (°C)	FWHM (deg.)	L (nm)	a (nm)
200	0.534	11.92	0.591
250	0.505	12.76	0.591
300	0.427	14.21	0.592

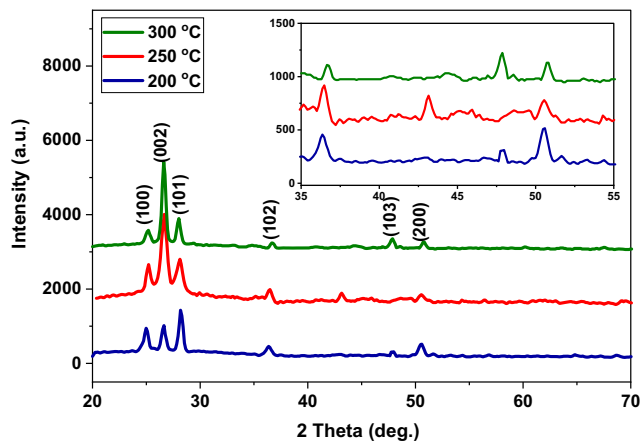


Fig. 3 XRD for CdS films prepared at different temperatures

Results and Discussion

Morphological Analysis

The surface morphology of films was characterized by utilizing FESEM technique, which generates topological images of surfaces at very high resolution. Figure 1 a, b displays the FESEM images of PbS and CdS thin films deposited on the ITO substrate at 300 °C. It is obvious that the nanoparticles have diverse size values; however, the geometry of the surface has a high degree of regularity. Figure 3 c, d displays a statistical distribution of the particle size over the surface and indicates that the value of the distribution occurs between 10 and 100 nm.

Structural Analysis

The X-ray spectra of the PbS films grown on ITO by CSP route at different temperatures are demonstrated in Fig. 2. The spectra show six peaks at $2\theta = 26.1^\circ$, 30.2° , 43.1° , 51.4° , 53.2° , and 62.5° , respectively, related to the (111), (200), (220), (311), (222), and (400) diffraction planes of the polycrystalline of lead sulfide cubic phase. This observation is close to the values of the standard data of JCPDS card (05-0592) as reported in the literature [25]. All the PbS spectra exhibit that the diffraction plane intensities of major peaks increased with increment temperature of the substrate, which may due to the increasing of crystallite size and thickness. The lattice constants (a) of cubic PbS thin films are depicted in

Table 2 XRD parameters for CdS thin films

temperature (°C)	FWHM (deg.)	L (nm)	a (nm)	c (nm)
200	0.654	15.33	0.412	0.664
250	0.783	12.05	0.412	0.666
300	0.547	16.17	0.412	0.668

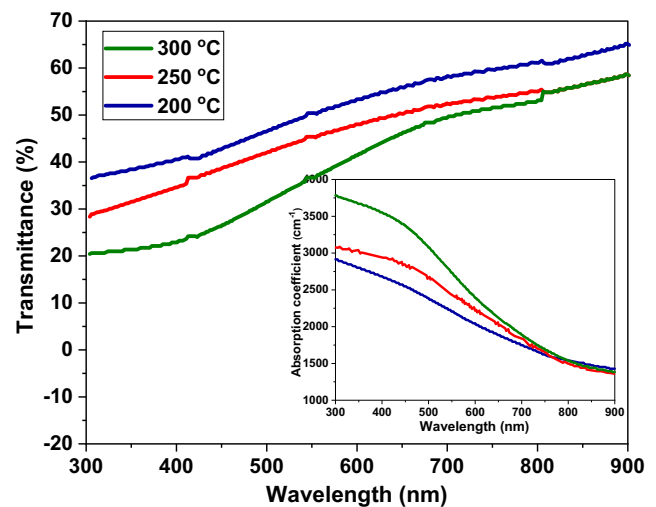


Fig. 4 Transmittance spectra for PbS films. Absorption coefficient variation (inset)

Table 1, and the estimated values were close to the standard lattice constant ($a_0 = 0.593$ nm). Figure 3 shows the X-ray spectra of CdS thin films formed on ITO by CSP method at different temperatures. The CdS thin films are appearing polycrystalline with a hexagonal phase. The intensive peaks are located at $2\theta = 24^\circ.8$, $26^\circ.52$, and $28^\circ.24$, which are corresponding to (100), (002), and (101) planes, respectively. Besides, other peaks with less intensity are centered at $2\theta = 36.6^\circ$, 47.8° , and 50.84° corresponding to (102), (103), and (200) planes, respectively, as reported in the previous work [26] (Table 2).

Optical Analysis

The UV-Vis transmittance spectra of the PbS and CdS films deposited at different temperatures are presented in Figs. 4 and 5, respectively. We notice that the PbS films have high transmission at high wavelengths (60–70%), and reducing to (20–

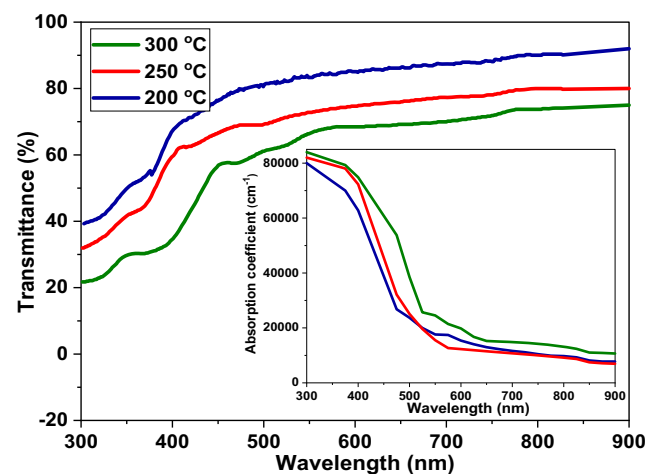


Fig. 5 Transmittance spectra for CdS films. Absorption coefficient variation (inset)

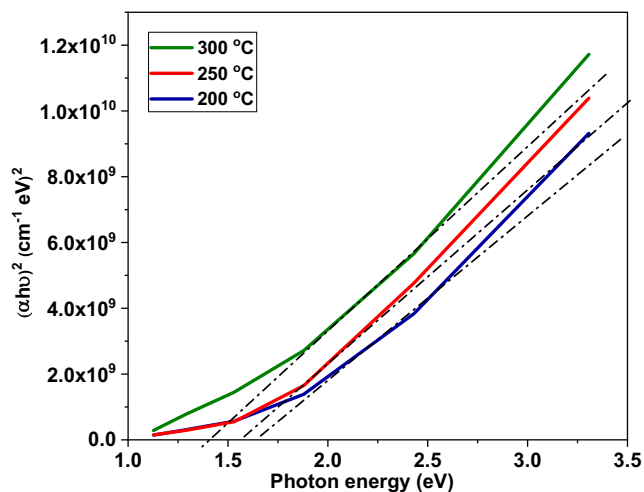


Fig. 6 Band gap for PbS thin films estimated by Tauc plot

30%) at low wavelengths. The transmittance spectrum of the PbS minimized with increment in substrate temperature; this may be the variation in particle size distribution from one sample to another [27]. On the other hand, the CdS films have high transparency in the visible region about 80% and sharp absorption band is appearing at 470 nm. All CdS film exhibits a window layer behavior of visible light, which is useful for optoelectronic applications [28]. The increase in transmittance of the films and CdS may be attributed to the less light scattering due to the better crystal structure and surface properties. The inset of Fig. 4 demonstrates the absorption coefficient recorded with wavelength for the PbS films at different substrate temperatures. It is clear that the PbS has a high absorption coefficient at the short wavelength range (300–550 nm), then reduces at different rates to reach constant values at long wavelengths which it is above (700 nm), where the films become transparent at this wavelength. The inset of Fig. 5 shows the absorption coefficient variation with wavelength for CdS film at different temperatures. Absorption coefficient increased slightly with substrate temperature; this may be due

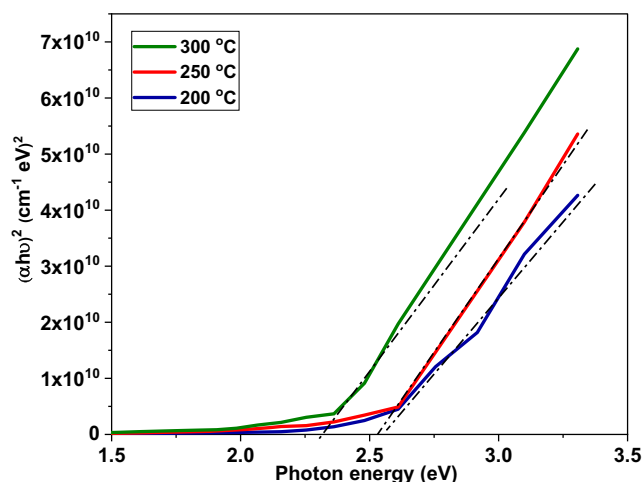


Fig. 7 Band gap for CdS thin films estimated by Tauc plot

Table 3 Energy gap variation with temperature for PbS and CdS thin films

Material	Temperature (°C)	E_g (eV)
PbS	200	1.65
	250	1.58
	300	1.4
CdS	200	2.57
	250	2.52
	300	2.31

to increasing of thickness and the degree of crystallization. The influence of the substrate temperature on the energy gap value of PbS and CdS films is shown in Figs. 6 and 7, respectively. As expected the increasing in the substrate temperature will lead to reduce in the magnitude of energy gap due to crystallization enhancement (see Table 3). These results are in good agreement with the references [29, 30]. The obtained band gap values for PbS are higher than the 0.42 eV reported for bulk PbS. In literature many authors have reported similar band gaps for films having small crystallite sizes [31]. It has been attributed to the quantum confinement. In the present study, the crystallite size is in the range of 10–14.5 nm, as determined from XRD patterns, which is smaller than the Bohr radius of PbS (18 nm). The decreasing dimension of the spherical crystallites might have influenced the density of states resulting in a red-shifting the fundamental absorption edge [32].

Electrical Measurements

Figure 8 presents the changing of capacitance with reverse bias voltage for ITO/CdS/PbS/Au heterojunction solar system produced in different thickness of the PbS film. A nonlinear reduces in capacitance with increment the reverse voltage; this resulted from alters of the width of the

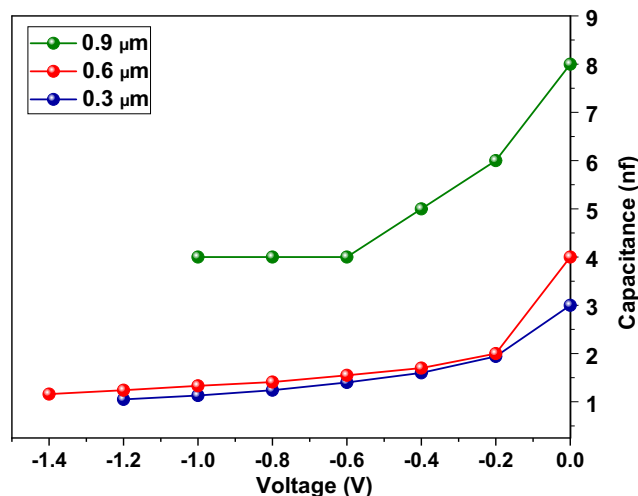


Fig. 8 C-V measurements for ITO/CdS/PbS/Au solar cell

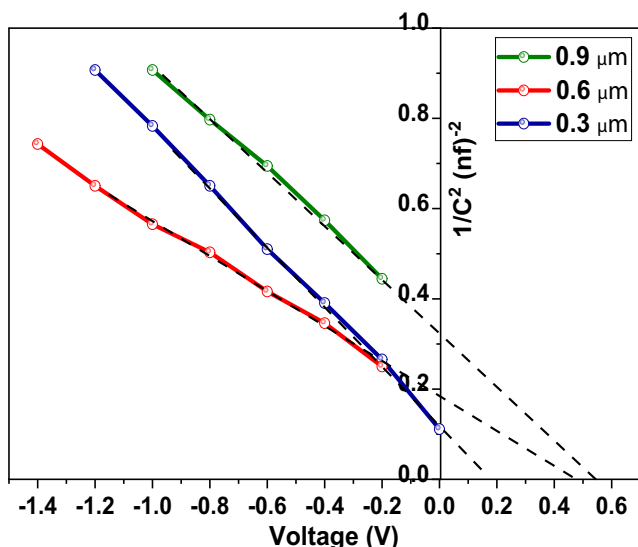


Fig. 9 Voltage versus $1/C^2$ for ITO/CdS/PbS/Au solar cell

depletion layer [33]. From Fig. 9, it is obvious that the V_{bi} becomes higher as the thickness of PbS film increases (see Table 4) due to more charge carriers present in thick PbS in comparison with thin PbS. The linear relation between $1/C^2$ and voltage suggests the abrupt kind of the heterojunction [34]. The PbS film represents absorber sheet, and its thickness plays a significant role, which controls the electrical measurements of the solar cells. J-V behavior of the ITO/CdS/PbS/Au heterojunction with different PbS thicknesses and under illumination is presented in Fig. 10. From Table 5, we notice that the high values of J_{SC} and V_{OS} was observed at the large thickness of the PbS film, because of a high absorption of radiation, which led to high photocurrent produced. The fill factor (FF) for solar cells can be measured via the below formula [35].

$$FF = \frac{J_m V_m}{J_{sc} V_{oc}}$$

From Table 5, we can see that the FF varies with the thickness of the PbS film. As the PbS thickness increases, the characteristics of the prepared solar cells enhanced; this can be ascribed to the decreasing of series resistance. The efficiency of the prepared solar cell was obtained by the following relation [35]:

Table 4 Built in potential for ITO/CdS/PbS/Au solar cell with different PbS thickness

Thickness of PbS (μm)	Built-in voltage (V)
0.3	0.18
0.6	0.49
0.9	0.54

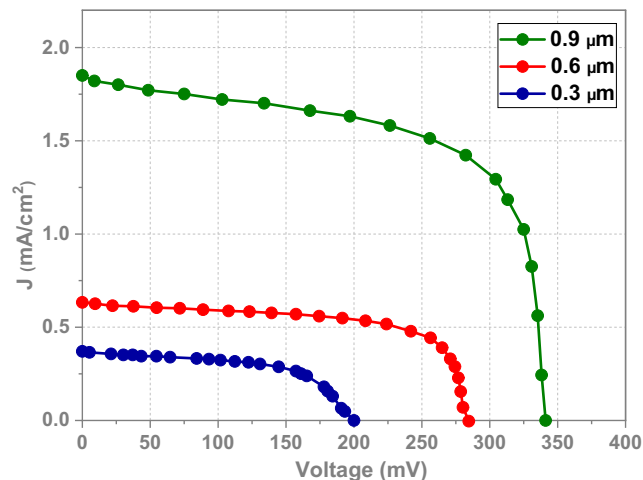


Fig. 10 J-V characteristic for ITO/CdS/PbS/Au solar cell

$$\eta = \frac{FF \times J_{sc} \times V_{oc}}{P_{light}}$$

From Fig. 10 and Table 5 it is clear that the short circuit photocurrent density (J_{sc}) of the cell has increased from 0.36 to 1.87 mA/cm^2 by increasing of absorber layer thickness, which is an impressive 50% increase. Correspondingly, the cell efficiency has also increased. The highest value of efficiency is around 0.85% of PbS thickness of 0.9 μm . The ITO/CdS/PbS/Au solar cell fabricated with 0.9 μm showed a dense and pinhole-free highly crystalline CdS/PbS film with improved optical and electrical properties. On the other hand, the ITO/CdS/PbS/Au solar cell fabricated with 0.3 μm suffered from low efficiency and severe recombination problems at the CdS/PbS interface. The comparison between the result obtained by another researcher and this study can be seen in Table 6. An improvement in solar cell performance can be attributed to an increment in light-harvesting ability and an enhancement in charge transport ability (reduction of charge recombination) at the CdS/PbS junction.

Conclusion

In order to obtain solar cell structures of ITO/CdS/PbS/Au, window (CdS) and absorption (PbS) layers have been

Table 5 Parameters of ITO/CdS/PbS/Au solar cells with different PbS thickness

Thickness of PbS (μm)	J_{SC} (mA/ cm^2)	V_{OC} (mV)	V_m (mV)	J_m (mA/ cm^2)	FF	η (%)
0.3	0.36	200	154	0.25	0.53	0.07
0.6	0.62	285	223	0.48	0.61	0.24
0.9	1.87	340	271	1.49	0.63	0.85

Table 6 Values of CdS/PbS solar cell efficiency for this study and previous studies

Researcher	Process for PbS	Intensity (mW/cm ²)	Obtained efficiency (%)
Kripal Singh [36]	CBD	100	No photovoltaic response
L. Pean-Cabrera et al. [37]	CBD	100	0.0335
CE Pérez-García et al. [38]	SILAR	100	0.127
Jayesh Patel et al. [25]	Spin coating	80	0.24
Result of this study	CSP	50	0.82
Ahmed.S. Obaid et al. [32]	CBD	40	1.35

sequentially synthesized on ITO substrates using the CSP method. The structural and optical properties of prepared thin films were strongly depended on the changing of substrate temperature. XRD proved that all thin films are polycrystalline. Using FESEM, the present work showed that the films have a uniform surface morphology over the substrate without pinholes or cracks. It was found that the performance of fabricated solar cell depended on the thickness of the absorber sheet (PbS). The output power density and the cell efficiency have been increased with increasing the thickness of absorber layer. The photovoltaic performance of the ITO/CdS/PbS/Au solar cells showed that the solar cell fabricated with thickness 0.9 μm of the PbS film exhibited higher efficiency of 0.85% including $J_{\text{SC}} = 1.87 \text{ mA/cm}^2$, $V_{\text{OC}} = 340 \text{ mV}$, and $\text{FF} = 0.63$ than the PbS film deposited with thickness 0.3 μm ($\eta = 0.07\%$, $J_{\text{SC}} = 0.36 \text{ mA/cm}^2$, $V_{\text{OC}} = 200 \text{ mV}$, $\text{FF} = 0.53$).

References

- Dissanayake MAKL, Liyanage T, Jaseetharan T, Senadeera GKR, Dassanayake BS (2020) Effect of PbS quantum dot-doped polysulfide nanofiber gel polymer electrolyte on efficiency enhancement in CdS quantum dot-sensitized TiO₂ solar cells. *Electrochim Acta* 347:136311. <https://doi.org/10.1016/j.electacta.2020.136311>
- Gode F, Unlu S (2019) Synthesis and characterization of CdS window layers for PbS thin film solar cells. *Mater Sci Semicond Process* 90:92–100
- Samadpour M, Jun HK, Parand P, Najafi MN (2019) CdS quantum dots pre-deposition for efficiency enhancement of quantum dot-sensitized solar cells. *Sol Energy* 188:825–830
- Rohom AB, Londhe PU, Jadhav PR, Bhand GR, Chaure NB (2017) Studies on chemically synthesized PbS thin films for IR detector application. *J Mater Sci Mater Electron* 28:17107–17113
- Rajashree C, Balu AR (2016) Tuning the physical properties of PbS thin films towards optoelectronic applications through Ni doping. *Optik* 127:8892–8898
- Hernández-Borja J, Vorobiev YV, Ramírez-Bon R (2011) Thin film solar cells of CdS/PbS chemically deposited by an ammonia-free process. *Sol Energy Mater Sol Cells* 95:1882–1888
- Obaid AS, Hassan Z, Mahdi MA, Bououdina M (2013) Fabrication and characterisations of n-CdS/p-PbS heterojunction solar cells using microwave-assisted chemical bath deposition. *Sol Energy* 89:143–151
- Dharmadasa IM, Bingham PA, Echendu OK, Salim HI, Druffel T, Dharmadasa R, Sumanasekera GU, Dharmasena RR, Dergacheva MB, Mit KA, Urazov KA, Bowen L, Walls M, Abbas A (2014) Fabrication of CdS/CdTe-based thin film solar cells using an electrochemical technique. *Coatings* 4:380–415
- Ahmed BA, Shallal IH, AL-Attar FIM (2018) Physical properties of CdS/CdTe/CIGS thin films for solar cell application. *IOP Conf Series J Phys Conf Series* 1032:012022
- Kartopu G, Turkay D, Ozcan C, Hadibrata W, Aurang P, Yerci S, Unalan HE, Barrioz V, Qu Y, Bowen L, Gürelek AK, Maiello P, Turan R, Irvine SJC (2018) Photovoltaic performance of CdS/CdTe junctions on ZnO nanorod arrays. *Sol Energy Mater Sol Cells* 176:100–108
- Abdallah B, Hussein R, Al-Kafri N, Zetoun W (2019) PbS thin films prepared by chemical bath deposition: effects of concentration on the morphology, structure and optical properties. *Iran J Sci Technol Trans Sci* 43:1371–1380
- Chaki SH, Joshi HJ, Tailor JP, Deshpande MP (2014) Study of SnS₂ thin film deposited by spin coating technique. *Mater Res Express* 4:076402
- Atwa D, Azzouz IM, Badr Y (2011) Optical, structural and optoelectronic properties of pulsed laser deposition PbS thin film. *Appl Phys B Lasers Opt* 103:161–164
- Khan MD, Hameed S, Haider N, Afzal A, Sportelli MC, Cioffi N, Malik MA, Akhtar J (2016) Deposition of morphology-tailored PbS thin films by surfactant-enhanced aerosol assisted chemical vapor deposition. *Mater Sci Semicond Process* 46:39–45
- Silva Filho JMC, Ermakov VA, Marques FC (2018) Perovskite thin film synthesised from sputtered lead sulphide. *Sci Rep* 8:1563
- Sarma MP, Wary G (2017) Effect of molarity on structural and optical properties of chemically deposited nanocrystalline PbS thin film. *Int Lett Chem Phys Astron* 74:22–35
- Romero R, Lpez M, Leinen D, Martin F, Ramos-Barrado J (2004) Electrical properties of the n-ZnO/ C-Si heterojunction prepared by chemical spray pyrolysis. *Mater Sci Eng B* 110:78–93
- Faraj MG (2015) Effect of thickness on the structural and electrical properties of spray pyrolysed lead sulfide thin films. *Am J Condens Matter Phys* 5:51–55
- Al-Mousoi AK, Mohammed MKA, Khalaf HA (2016) Preparing and characterization of indium arsenide (InAs) thin films by chemical spray pyrolysis (CSP) technique. *Optik* 127:5834–5840
- Ahmed DS, Mohammed MKA, Mohammad MR (2020) Sol-gel synthesis of Ag-doped titania-coated carbon nanotubes and study their biomedical applications. *Chem Pap* 74:197–208
- Mohammad MR, Ahmed DS, Mohammed MKA (2019) Synthesis of Ag-doped TiO₂ nanoparticles coated with carbon nanotubes by the sol-gel method and their antibacterial activities. *J Sol-Gel Sci Technol* 90:498–509
- Mohammed MKA, Ahmed DS, Mohammad MR (2019) Studying antimicrobial activity of carbon nanotubes decorated with metal-doped ZnO hybrid materials. *Mater Res Express* 6:055404
- Raneen IJ, Mohammed MKA (2016) Production of graphene powder by electrochemical exfoliation of graphite electrodes immersed in aqueous solution. *Optik* 127:6384–6389

24. Mohammed MKA, Ali KA, Haider AK (2016) Deposition of multi-layer graphene (MLG) film on glass slide by flame synthesis technique. *Optik* 127:9848–9852
25. Patel J, Mighri F, Ajji A, Tiwari D, Chaudhuri TK (2014) Spin-coating deposition of PbS and CdS thin films for solar cell application. *Appl Phys A Mater Sci Process* 117:1791–1799
26. Saikia D, Phukan P (2014) Fabrication and evaluation of CdS/PbS thin film solar cell by chemical bath deposition technique. *Thin Solid Films* 562:239–243
27. Khare A (2010) Effects of copper concentration on electrooptical and structural properties of chemically deposited nanosized (Zn-Cd) S:Cu films. *J Lumin* 130:1268–1274
28. Spalatu N, Hiie J, Mikli V, Krunk M, Valdna V, Maticiu N, Raadik T, Caraman M (2015) Effect of CdCl₂ annealing treatment on structural and optoelectronic properties of close spaced sublimation CdTe/CdS thin film solar cells vs. deposition conditions. *Thin Solid Films* 582:128–133
29. Kumarasinghe OK, Dissanayake A, Pemasiri BM, Dassanayake BS (2017) Thermally evaporated CdTe thin films for solar cell applications: optimization of physical properties. *Mater Res Bull* 96: 188–195
30. Cruz JS, Perez RC, Delgado GT, Angel OZ (2015) CdS thin films doped with metal-organic salts using chemical bath deposition. *Thin Solid Films* 518:1791–1795
31. Droessler LM, Assender HE, Watt AAR (2012) Thermally deposited lead oxides for thin film photovoltaics. *Mater Lett* 71:51–53
32. Obaid AS, Mahdi MA, Hassan Z, Bououdina M (2012) Preparation of chemically deposited thin films of CdS/PbS solar cell. *Superlattice Microst* 52:816–823
33. Shin SW, Agawane GL, Gang MG, Moholkar AV, Moon JH, Kim JH, Lee JY (2012) Preparation and characteristics of chemical bath deposited ZnS thin films: effects of different complexing agents. *J Alloys Compd* 526:25–30
34. Altin I, Polat I, Bacaksiz E, Sokmen M (2012) ZnO and ZnS microrods coated on glass and photocatalytic activity. *Appl Surf Sci* 258:4861–4865
35. Artegiani E, Menossi D, Salavei A, di Mare S, Romeo A (2017) Analysis of the influence on the performance degradation of CdTe solar cells by the front contact. *Thin Solid Films* 633:101–105
36. Singh K (2014) PbS-CdS thin film heterojunctions for photovoltaic applications, a thesis submitted to School of Physics and Materials Science. Thapar University, Patiala
37. Peña-Cabrera L, Arizmendi-Morquecho A, Vorobiev P (2016) Thin film CdS/PbS solar cell by low temperature chemical bath deposition and silver doping of the window layer. *J Non-Oxide Glas* 8:59–66
38. Pérez-García CE, Meraz-Dávila S, Arreola-Jardón G, de Moure-Flores F, Ramírez-Bon R, Vorobiev YV (2020) Characterization of PbS films deposited by successive ionic layer adsorption and reaction (SILAR) for CdS/PbS solar cells application. *Mater Res Express* 7:015530

Publisher's Note Springer Nature remains neutral with regard to jurisdictional claims in published maps and institutional affiliations.